城市场景时序 InSAR 形变解译问题分析与研究进展

Yang, Mengshi; Liao, Mingsheng; Chang, Ling; Hanssen, Ramon F.

DOI
10.13203/j.whugis20230289

Publication date
2023

Document Version
Final published version

Published in
Beijing Ligong Daxue Xuebao/Transaction of Beijing Institute of Technology

引文格式:杨梦诗,廖明生,常玲,等.城市场景时序InSAR形变解译:问题分析与研究进展[J].武汉大学学报(信息科学版),2023,48(10):1643-1660.DOI:10.13203/j.whugis20230289

Citation:YANG Mengshi,LIAO Mingsheng,CHANG Ling,et al.Interpretation of Multi-epoch InSAR Deformation for Urban Scenes:A Problem Analysis and Literature Review[J].Geomatics and Information Science of Wuhan University,2023,48(10):1643-1660.DOI:10.13203/j.whugis20230289

城市场景时序InSAR形变解译:问题分析与研究进展

杨梦诗[1] 廖明生[2] 常 玲[3] Ramon F. Hanssen[4]

1 云南大学地球科学学院,云南 昆明,650500

2 武汉大学测绘遥感信息工程国家重点实验室,湖北 武汉,430079

3 University of Twente, Faculty of Geoinformation Science and Earth Observation, Enschede, The Netherlands, 7522NH

4 Delft University of Technology, Department of Geoscience and Remote Sensing, Delft, The Netherlands, 2628CN

摘 要:时序InSAR(interferometric synthetic aperture radar)技术可以提供周期性形变监测,已经广泛应用于地表沉降和基础设施形变监测等工作,为城市安全和可持续发展提供重要保障。然而,由于城市场景的复杂性,InSAR精细监测以及形变信号解译仍然是一个难题和挑战。从时序InSAR相干点与地物目标映射关系不确定性为切入点,剖析了这种不确定性带来的形变解译问题,包括:(1)精细形变监测,即形变信号"在哪里";(2)形变机制和驱动因素认知,即形变信号"是什么";(3)形变信号对观测事件的反映,即考虑城市场景下的合成孔径雷达信号的复杂散射机制。引入了时序InSAR监测体系下InSAR相干点的描述框架,包括运动学特征、几何参数、语义信息、物理属性,并回顾了InSAR相干点参数提取与形变解译的研究进展。基于InSAR相干点几何参数、语义信息、物理属性的综合形变解译与机制认知将是未来城市场景精细形变监测、识别和安全评估等服务的关键。

关键词:时序InSAR技术;InSAR相干点;城市形变监测;InSAR形变解译

中图分类号:P237 **文献标识码**:A **收稿日期**:2023-08-05

DOI:10.13203/j.whugis20230289 **文章编号**:1671-8860(2023)10-1643-18

Interpretation of Multi-epoch InSAR Deformation for Urban Scenes: A Problem Analysis and Literature Review

YANG Mengshi[1] *LIAO Mingsheng*[2] *CHANG Ling*[3] *HANSSEN Ramon F.*[4]

1 School of Earth Sciences, Yunnan University, Kunming 650500, China

2 State Key Laboratory of Information Engineering in Surveying, Mapping and Remote Sensing, Wuhan University, Wuhan 430079, China

3 University of Twente, Faculty of Geoinformation Science and Earth Observation, Enschede, The Netherlands, 7522NH

4 Delft University of Technology, Department of Geoscience and Remote Sensing, Delft, The Netherlands, 2628CN

Abstract: Multi-epoch interferometric synthetic aperture radar (InSAR) is a highly effective technique for monitoring deformation in urban areas. However, interpreting InSAR deformation can be challenging due to various factors, including inherent geometric imaging distortion, the intricate structure and deformation properties of targets in urban scenes, and the multiple scattering of microwave signals between objects in urban scenes. This paper discusses the challenges involved in interpreting time-series InSAR deformation: (1) Precisely identifying the location of deformation signals and linking them to their corresponding objects, i.e., determining where the deformation signal occurs, (2) understanding the mechanisms and factors that cause the detected deformation signals, i.e., determining what the deformation signal represents, (3) establishing the connection among the detected deformation signals, the deformation events, and the scattering

基金项目:国家自然科学基金(42101450);云南省基础研究计划(202201AU070014, 202301AT070145);武汉大学测绘遥感信息工程国家重点实验室开放基金(21R03);云南省"兴滇英才"青年人才引进项目。

第一作者:杨梦诗,副教授,研究方向为时间序列InSAR算法及其在地表形变监测中的应用。yangms@ynu.edu.cn

通讯作者:廖明生,博士,教授。liao@whu.edu.cn

mechanisms. We suggest a parametric framework to improve the accurate interpretation of InSAR deformation. This framework includes several factors, including kinematic characteristics (deformation rate, cumulative deformation, deformation gradient, and deformation model), geometric parameters (position, size, structure, orientation, and roughness), semantic information (land cover type, terrain morphology, texture, and auxiliary information on natural and anthropogenic disturbance) and physical properties (scattering mechanism, penetrability, extensibility, conductivity, and thermal conductivity). Our approach aims to enhance the representation of coherent points for a better understanding of InSAR deformation. This paper offers a comprehensive overview of the advancements achieved in extracting parameters of InSAR coherent points and interpreting deformation based on geometric parameters, semantic information, and physical properties. High-precision 3D positioning is crucial for InSAR fine monitoring in urban areas. It helps determine the source of deformation signals and facilitates the analysis of deformation mechanisms. Semantic information, such as 3D models, high-resolution optical images, laser point cloud data, and land use data, can aid in interpreting InSAR deformation. By combining InSAR deformation data with a deep learning approach, there is an opportunity to interpret deformations effectively. In urban environments, the scattering mechanism of ground objects is complex. Multiple scattering signals can provide effective observations of deformation and information about the target's size. However, combining the scattering mechanism of synthetic aperture radar signals to carry out parameter inversion and deformation mechanism interpretation of urban target terrain remains a challenge. The framework, which considers the geometric parameters, semantic information, and physical attributes of InSAR coherent points, will be crucial for deformation interpretation and mechanism cognition. This framework will enable fine deformation monitoring, intelligent recognition, and application in future urban scenes.

Key words: time series InSAR technique; InSAR coherent point; urban deformation monitoring; InSAR deformation interpretation

受世界人口增长、设施老化和地面/土壤动态变化的影响,城市的基础设施健康状况正受到越来越多的关注。基础设施存在的使用年限,其状况极易受到人类活动如地下水抽取、矿物开采和隧道修建等生产建设过程,以及自然过程如地陷、海平面上升等地质环境变化的影响。因此,对城市建筑进行长期持续的监测,及时捕捉到异常的形变信号是保障城市设施安全运维和可持续发展的重要保障。

基于点位观测的传统大地测量方法需要重复地对每一座设施及其细部结构展开测量,费时费力,且成本高。合成孔径雷达干涉测量(interferometric synthetic aperture radar, InSAR)则是利用雷达回波的相位信息来精确地测量地物三维空间位置及其微小变化,具有全天时、全天候地提供大范围地表观测的工作能力,可为长期性的广域形变监测发挥重要作用。尤其是时序InSAR技术[1-5]的出现,它克服了InSAR技术受去相干和大气干扰的限制,利用在长时间观测下依然能提供可靠相位信息的点目标开展形变提取,使得应用InSAR开展城市地表形变信息提取的技术跨入了新时代[6]。

早期研究关注于城市大范围的地表沉降,欧洲航天局(European Space Agency, ESA)的ERS-1/2和ENVISAT ASAR、日本宇宙航空研究开发机构(Japan Aerospace Exploration Agency,JAXA)的JERS-1、加拿大国家航天局(Canadian Space Agency,CSA)的Radarsat-1等雷达卫星数据为初期研究提供了大量的数据[7],促进了InSAR城市监测应用的相关理论方法和应用技术的迅速发展,自2014年ESA的Sentinel-1 A/B数据的业务化运行,提供了后续大批量开源周期性观测的合成孔径雷达(synthetic aperture radar, SAR)数据,充分推动了中国先后在北京[8-9]、天津[10-11]、上海[12-14]、西安[15-16]、太原[17-18]、广州[19-21]、武汉[22-23]、苏州[24-25]等地开展了其应用研究和业务推广工作[26-28]。第二代高分辨率星载SAR系统,包括德国宇航中心(Deutsches Zentrum für Luft- und Raumfahrt, DLR)的TerraSAR-X/TanDEM-X、意大利航天局的COSMO-SkyMed星座组、CSA的Radarsat-2、JAXA的ALOS-1/2 PALSAR-1/2任务的开展,雷达卫星影像的分辨率由十余米提高到了米级(条带模式)甚至亚米级(凝视聚束模式),使得雷达遥感技术真正进入

了高分辨率时代,在城市地表形变的精细化监测方面展现出了巨大的潜力,为机场[29-34]、桥梁[35-41]、铁路和高速公路[42-46]、地铁[47-55]、建筑物[56-64]等城市基础设施的监测提供有力保障。随着中国 GF-3 和 LT-1、西班牙 PAZ、阿根廷 SAOCOM、韩国 KOMPSAT-5、印度 RISAR-1,以及下一代 COSMO-SkyMed、Radarsat 星座组、TanDEM-L、ESA Sentinel-1 C/D、BIOMASS、Harmony 美国 NISAR 等卫星任务的运营和计划,多平台、多波段、多极化、多分辨率、多角度的 SAR 数据提供了地表丰富的信息数据。SAR 数据中可以获取的地物信息越来越丰富,然而城市场景中克服目标的复杂性、建筑物之间的多次散射特性以及 SAR 数据固有的几何畸变特征,在大数据时代利用星载 SAR 卫星数据实现成像和识别一体化[65-67],从而实现复杂城市场景的 InSAR 精细监测以及形变信号解译依然是当前以及未来的挑战。

1　城市场景 InSAR 形变解译问题解析

数据驱动的时序 InSAR 分析方法,聚焦于长时序具有可靠相位观测的高相干点实现高精度形变估计。时序 InSAR 技术的相干点,即人们观测的点目标,是在一组 SAR 数据中选取保持高相干特性的信号点,属于后验选点。不同于大地测量技术中的观测点,如水准测量中的标点,是事先选取的、具有准确的空间位置和明确的物理含义的目标,可最大程度地发挥测量结果的作用[68]。

图 1 展示了典型的时序 InSAR 形变监测结果示例,该结果是 2014—2017 年间荷兰鹿特丹区域 49 景 TerraSAR-X 的平均形变速率。每一个点代表了从时序 SAR 数据中选取的 InSAR 相干点。InSAR 相干点提供了高精度(毫米级)形变测量结果,然而 InSAR 相干点-地物目标-观测场景对应的不确定,使得形变信号起源识别、形变机制解译具有挑战,而正确解译形变信号正是 InSAR 进一步业务化推广应用的关键环节。

InSAR 相干点-地物目标-观测场景之间的不确定带来的问题体现在 3 个层次:

1)形变信号“在哪里”?考虑的是 InSAR 相干点的几何参数,即高精度的三维坐标位置。一般来说,时序 InSAR 相干点的三维定位精度低,约为几米到几十米[69]。如果能够提高 InSAR 相干点的三维位置精度,最直接的体现就是能准确找到出现变形信号的地物,甚至精确到单个地物的细部亚结构,无疑能够提升对于单个地物及结构细节的监测能力,对于形变信号的起源识别十分重要。

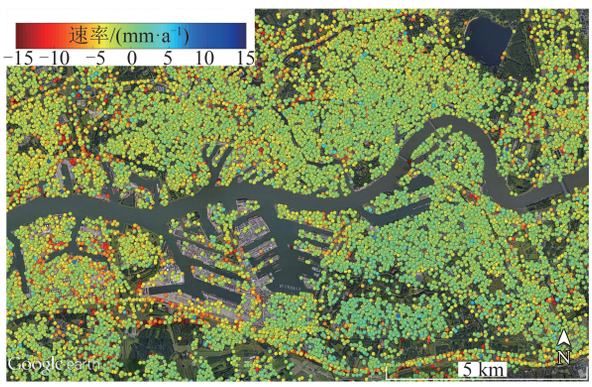

图 1　时间序列 InSAR 技术的典型结果(荷兰鹿特丹市 2014—2017 年 TerraSAR-X 数据速率图)

Fig. 1　A Typical Result by Time Series InSAR Technique(Mean Displacement Velocity Map Between 2014 and 2017 in the City of Rotterdam, the Netherlands from 49 TerraSAR-X Images)

2)形变信号“是什么”?这里考虑的是 InSAR 相干点所测量形变语义信息,即通过地物类型、地形地貌数据、自然和人为扰动等辅助信息和数据挖掘方法等,实现形变信号相关的形变机制的判别。在涉及多种形变机制的复杂场景中,InSAR 结果的解译更加重要。例如,监测地下工程活动引起的地面沉降事件时,可能表现为拥有稳固地基的建筑物上探测的相干点没有形变信号,而来自地面的相干点出现沉降信号。利用来自不同地物上的相干点形变信号的异同,可以揭示和判识形变信号背后的机制和驱动因素。

3)探测的形变信号“如何反映”真实的形变量级?这里考虑的是 InSAR 相干点的物理属性,即探测的形变信号受电磁散射机制以及地物本身物理特性响应的函数。雷达信号在复杂城市场景中存在多次散射,使得 InSAR 相干点的形变解读更为复杂。例如,由地面-建筑物-建筑物-地面四次散射点的信号,形成建筑物的“重影”散射点,其探测到的形变信号与建筑物真实形变存在差异。此外,同样作为二次散射信号,由建筑物自身亚结构形成的二次散射信号与建筑物和地面形成的二次散射信号,它们所测量的形变信号也应分别对待。因此,散射机制是 InSAR 相干点形变的解译不可忽略的因素,InSAR 所探测的形变信号需要结合其物理属性讨

论。例如,针对建筑物的形变监测中,要考虑建筑物本身热膨胀效应带来的形变信号,才能准确识别形变异常信号。InSAR相干点物理属性的确定,需要结合几何参数以及语义信息讨论,如建筑物本身的二次散射信号和由建筑物和地面形成的二次散射信号的形变可以结合散射点的精密三维空间位置和散射机制来分析,对于城区不同材料的地物的形变可以结合其导热系数与地物类型来分析。

图2尝试总结了当前建立InSAR相干点-地物目标-观测场景之间的关联的关键参数,主要包含4个方面:(1)运动学特征,包含形变速率、形变位移量、形变梯度、形变模型;(2)几何参数,包含空间坐标位置、尺寸结构、空间朝向和粗糙度;(3)语义信息,包括地物类型、地形地貌、纹理和自然人为扰动辅助信息;(4)物理属性,包括散射机制、穿透性、延展性、导电和导热性。InSAR相干点的运动学特征参数即时序InSAR技术所反演的相关形变参数,本文的后续章节将重点讨论InSAR相干点几何参数、语义信息和物理属性提取以及对于InSAR形变信号解译相关研究的进展。

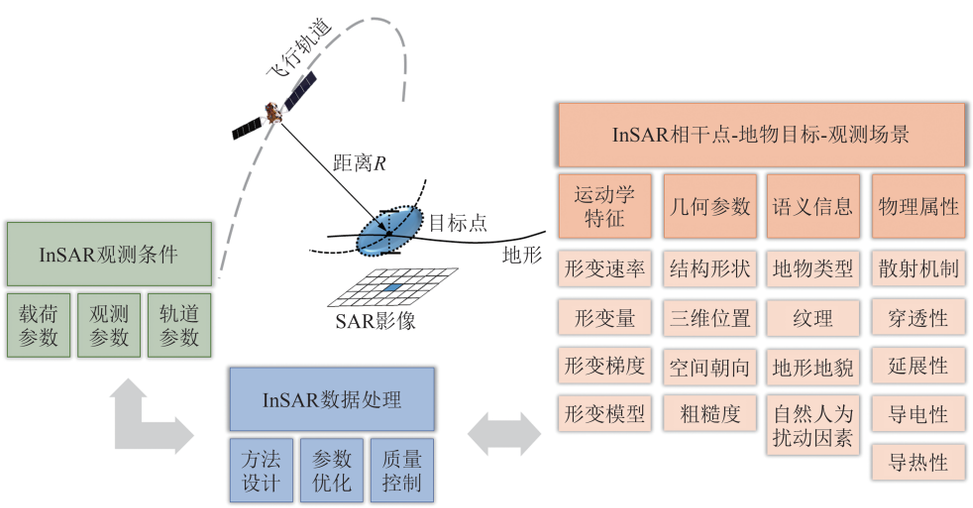

图2 时序InSAR监测体系下城市场景InSAR观测目标的不确定性

Fig. 2 Uncertainty of InSAR Observation Targets in Urban Scenarios Using Time Series InSAR Techniques

2 复杂城市场景InSAR相干点参数提取与形变解译研究进展

2.1 InSAR相干点几何参数提取与形变解译

建立InSAR相干点-地物目标-观测场景之间的关联,最直接的和关键的参数即InSAR相干点三维空间位置。InSAR几何参数中空间朝向和粗糙度是相对于传感器而言的,尺寸结构在形变解译中则多作为辅助信息来使用,而精密的三维空间位置则是回答形变信号“在哪里”以及进一步讨论形变信号“是什么”的关键。本节重点关注InSAR相干点的几何参数空间位置确定,即InSAR相干点定位处理,以及联合空间位置的形变解译研究进展。

2.1.1 InSAR相干点精密定位

InSAR相干点位置的精度主要受5个方面的因素影响,包括传感器相关的误差、传播过程误差(大气效应)、地球动力因素、参考点误差和坐标转换误差,如图3所示。因此,已有的InSAR相干点精密定位的研究主要分为三类:(1)针对定位过程中各项误差的改正;(2)雷达多基线测量/雷达摄影测量/立体SAR方法;(3)借助于外部参考点/数据的改正方法。下面主要从这三方面来总结近年来关于InSAR相干点精密定位的主要研究概况和各个方法的特点。

针对定位过程中各项误差改正的方法,涉及定位过程中各类误差的校正,包括方位偏移[70]、大气路径延迟(path delay, PD)[71]、板块构造运动[71]、固体地球潮汐(solid earth tide, SET)和极移(polar motion, PM)[71]等。Eineder等[72]指出对流层水汽变化和SET是SAR距离测量中最大的误差源,通过校正PD、SET和PM,利用TerraSAR-X高分辨率聚束模式(spotlight, ST)数据实现了3.8 cm的距离向和5.6 cm的方位向定位精度,并提出SAR影像大地测量

概念。Cong 等[73]通过数值天气模型的 PD 估计和大陆漂移补偿，进一步将精度从 3.8 cm 提高到 3.2 cm。Balss 等[74]总结了地球动力学影响的校正，将 TerraSAR-X ST 数据的绝对定位精度提高到厘米级。在 2014 年 Sentinel-1A 数据调试阶段，研究人员通过校正 PD、SET 和双基地残差后，发现图幅模式数据（stripmap，SM）有 1.8 m 的方位向定位偏差，可能来源于仪器设备时间偏差、轨道估计与插值精度、天线相位中心偏差或沿轨道运动的相对多普勒校正偏差等。

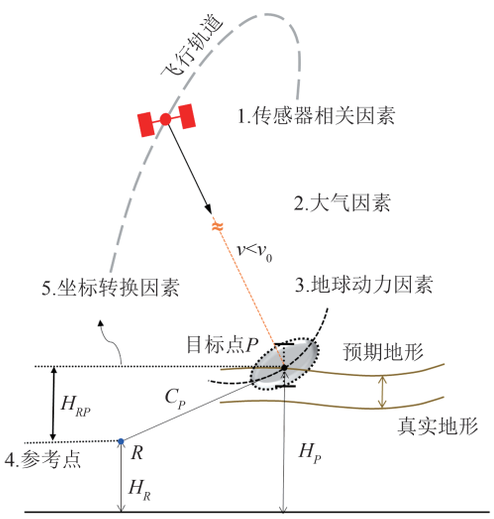

图 3　InSAR 相干点定位误差示意图

Fig. 3　Schematic Diagram of InSAR Coherent Point Positioning Errors

这样的方位向定位偏差同样在干涉宽幅模式数据（interferometric wideswath，IW）中被发现，且随着斜距增大，被称为 Sub-swath 依赖的方位向偏差[75]。这项研究给出的结果显示通过校正各类误差项获得的绝对定位精度是远高于 Sentinel-1 SM 数据（2.5 m）和 IW 数据（7 m）的定位规范标准。需要注意的是，逐一地改正定位过程中的各项误差，对定位过程中误差的理解和针对每一项误差改正方法也很重要，否则会引入新的校正误差。2021 年，DLR 和苏黎世大学的团队同时利用澳大利亚角反射器序列作为验证[76]，两个团队对 SAR 几何定位误差有相同的理解，认为需要改正对流层和电离层延迟 PD、SET、二阶潮汐影响（海洋潮、极潮汐、海洋潮汐荷载、大气潮汐荷载、大气压强荷载）、地壳运动、双站的方位向偏差等。然而，两者在计算大气延迟的方法不同，最终结果显示对于 Sentinel-1 IW 数据的距离向定位精度结果相差 13 cm[76]。目前，这类研究集中在二维雷达坐标系内的处理，即只考虑方位向和距离向的绝对定位精度。表 1 列出了定位中主要误差的贡献量级，其中电离层延迟以 TerraSAR-X 数据为例。InSAR 相干点的精密定位更需要考虑从二维雷达坐标到三维大地坐标的问题。Gernhardt 等[77]对相干点的三维定位精度进行评估，发现 TerraSAR-X ST 数据中相干点的精度在方位和距离向都在厘米级，在高程向上从几分米到 1.8 m 不等。

表 1　精密定位各项误差的量级

Tab. 1　Magnitude of InSAR Positioning Errors

定位误差项	方位向	距离向	误差项量级大小
方位向偏移	dm - cm	—	高达厘米级
对流层延迟	—	m	2.5～3.5 m
电离层延迟	—	cm	1～20 cm
地球固体潮	cm	dm	－20～20 cm
海洋潮	mm	＜cm	高达 10 cm
海洋极潮荷载	mm	mm	高达 2 mm
大气潮汐荷载	mm	mm	高达 2 mm
大气压强荷载	mm	＜cm	高达 4 cm
地壳运动	dm	dm	高达分米级
极潮汐	mm	mm	高达厘米级

雷达多基线测量方法包含时序永久散射体 InSAR（persistent scatterer InSAR，PS-InSAR）方法、立体 SAR 或者雷达摄影测量的方法。雷达摄影测量方法出现较早，是源于摄影测量学中立体像对的方法[78]。这些方法主要是利用不同观测视角差异，实现 InSAR 相干点的三维定位。Gernhardt 等[79]提出一种几何融合方法实现多轨道数据的融合。Gisinger 等[80]使用立体 SAR 技术并联合改正 PD 和相关地球动力学效应，实现了厘米级的三维定位精度。Duque 等[81]通过一对 TerraSAR-X ST 图像进行离焦分析和立体测量处理，实现了亚米级地理定位精度。Zhu 等[82]结合 SAR 成像大地测量学[72]、立体 SAR[80]和层析 SAR[83]，构建一种三维定位的方法。同样地，Montazeri 等[84]结合 PS-InSAR 和 SAR 成像大地测量学[72]，实现了水平方向和垂直方向分别约 40 cm 和 20 cm 的定位精度。多轨道融合/立体 SAR 的方法能改善相干点三维定位精度，但要求观测场景能提取到从不同观测视角都可见的同一控制点，这通常对场景和数据分辨率有要求。已有研究几乎都是利用高分辨率 TerraSAR-X Spotlight 模式的数据。

雷达人工目标一般指被动的角反射器(corner reflector, CR)和主动式应答器,它已被广泛用于SAR系统的外部辐射定标[85-88]、低相干区的形变测量[89-93]、InSAR测量和定位的精度评估[76,94-96]、校正传感器的定时偏移[87]。雷达人工目标具有高且稳定的雷达散射截面(radar cross section, RCS)和定义明确的散射相位中心,使得其能在SAR影像中准确识别。借助于地面控制点进行几何校正在摄影测量领域很常见。在InSAR精密定位中,利用雷达人工目标作为精密定位的控制点,提供InSAR精密定位的改正是当前研究趋势。

Gisinger等[80]利用角反射作为控制点实现了高精度立体的三维定位,之后该团队研究了多方向视角的小反射器的立体定位[97]。Mahapatra等[98]利用主动式雷达应答器,实现了InSAR和全球导航卫星系统数据的测量基准关联。Yang等[99]提出利用单个角反射器在单景SAR影像和在时间序列SAR影像(Multi-epoch CR)的定位改正方法,对比于地球物理参数改正和激光点云辅助改正方法,Multi-epoch CR方法获得了最高的精度,在TerraSAR-X SM和Sentinel-1 IW数据的三维定位精度分别约0.6 m和3 m。Gisinger等[100]首次给出在主动式雷达应答器上Sentinel-1数据的定位精度,发现主动式应答器在方位向上结果较好,但是距离向上不如被动式角反射器,且主动式雷达应答器的形变相位观测还需要矫正。Eineder等[101]展示了Sentinel-1的被动和主动反射器定位结果,发现主动式反射器有较高RCS,但其距离向定位精度约12 cm,低于被动反射器约1~5 cm的精度。

除了利用角反射器作为控制点的定位辅助的方法,激光雷达获取的高精度点云数据也能辅助InSAR相干点的精密定位。Chang等[58]分析了地面激光点云和InSAR地面点高程数据分布差异计算InSAR参考点高程偏差,实现InSAR点云全局定位的校准。同样地,Yang等[102]利用一个角反射器和三维激光点云数据联合实现了TerraSAR-X的三维定位改正。Yang等[99]提出了一种基于InSAR定位误差椭圆加权的迭代最近点点云匹配方法,借助于高精度激光点云数据,在TerraSAR-X SM数据和Sentinel-1 IW数据中的三维定位精度分别约1.6 m和4.5 m。Liu等[62]提出基于激光点云数据改正不同平台InSAR相干点的定位误差,从而实现城市建筑的形变监测。利用已有的高精度激光点云开展定位改正,相当于有大量的地面控制点参与定位误差改正的最优估计,是非常高效的方法,也是今后的发展趋势。

InSAR相干点三维高精度定位需要充分考虑定位过程中各项误差。关于不同定位方法的计算效果以及使用条件方面的对比,可以参考文献[99]。针对各项地球动力学因素改正的方法,难以解决参考点的高程偏差问题。结合多轨道视角的方法对数据分辨率和观测场景有一定要求。利用高精度控制数据,包括雷达人工目标的大地测量数据或高精度激光点云数据是InSAR定位精度改正的重要途径,但发展无地面控制点InSAR点云精密三维定位方法则是未来技术突破的关键。

2.1.2 联合InSAR相干点精密定位的形变解译

InSAR相干点的位置信息建立了与地物目标关联的重要基础数据。从InSAR相干点的高程信息出发,可以将城市场景内探测的InSAR相干点分为地面点和具有高度的点(建筑物、高架桥)。Dheenathayalan等[103]对比了基于幅度、高程和极化信息的InSAR相干点分类方法,并指出相比于结合幅度(90%)方法,基于高程的分类方法能达到89%的正确率,证明了高程信息在地物分类的重要性。基于高程信息的InSAR相干点分类,提取有一定高程值的相干点集[38-39,44,104],可以实现建筑物、高架路、桥梁等目标的监测。在一定场景条件下,高程提供的信息也可以作为语义信息转化,来自不同地物目标的InSAR相干点的形变信号的差异分析,实现对建筑形变、浅层形变、深层形变等相关信号的解译[55]。InSAR精密的空间位置作为重要的参数信息,是与其他数据融合的前提,也是后续开展基础设施精细化监测的基础,如高层建筑物的倾斜度评估,桥梁结构健康监测等等,从而提供地物目标的形变解译所需的深层信息。

2.2 时序InSAR形变语义信息解译

精密的三维空间位置回答了形变信号“在哪里”,本节关注的是形变信号“是什么”,即揭示和判识形变信号背后的机制和驱动因素的关键。从InSAR相干点目标的特征出发,通过地物类型、地形地貌数据、辅助信息等,实现形变信号相关的形变的解读,是从InSAR相干点语义信息出发的形变信号解译。另一方面从InSAR形变数

据本身出发,以数据驱动的方法开展形变信号解译。本节将从这两方面回顾和总结相关研究进展。

2.2.1　基于 InSAR 相干点语义信息的形变解译

借助于外部数据确定 InSAR 相干点的语义信息,包括高分辨率光学遥感影像、激光点云数据和三维建筑模型等等,从而整合外部数据的语义信息实现 InSAR 目标识别和形变解译。这类方法需要顾及不同数据之间的匹配和转换关系。Wang 等[105]借助于光学遥感影像,主要考虑不同成像差异特征来实现从光学影像提供的标签信息的迁移。同样的,借助于地表覆盖产品也能提供 InSAR 形变解译的辅助信息[106],关键在于雷达数据与外部数据之间匹配。此外,InSAR 相干点可以看作一种广义的点云数据,假设 InSAR 数据和激光数据的穿透性接近,而激光点云数据具备的丰富语义信息可辅助解译 InSAR 点云数据信息[107]在顾及两种数据定位精度差异的情况下,引入激光点云的标签信息,实现了铁路沿线的相干点分类以及形变的解译。通过建筑物的轮廓数据可以建立 InSAR 点云与单个建筑物关联[108-109],随着城市三维建筑模型可用产品增加,基于高精度的 InSAR 定位结果与建筑模型的可视化,能提供直接的 InSAR 结果解译产品[77,108,110]。

2.2.2　基于数据驱动的 InSAR 的形变解译

基于数据驱动的形变信号解译,一方面是从形变数据的信息挖掘,以形变信号空间和时间特性分析为基础,深入理解形变信号。考虑城市区域形变的混叠特征,在频率域分解区域形变和局部形变信号[12,106,111],将地表沉降带来的大尺度空间形变信号和局部工程影响叠加的局部形变信号分解,有利于局部异常探测。城市场景下多种形变的混叠,引入智能聚类算法在大数据 InSAR 形变点云中确定具有相似形变特性类别,能实现大范围形变的快速解译[112-114]。InSAR 形变的运动学特征可以提供形变演化的信息,将 InSAR 的时序形变信号分解为周期分量和分段线性分量,周期分量表示目标由于季节影响而产生的规律变形,分段线性分量表示不同时期的变形趋势[115-116]。InSAR 形变的运动学特征也可以利用统计检验方法分为线性型、温度型、指数型、阶梯型等[117-118]。

另一方面是建立专家知识形变信号库,引入深度学习的方法实现智能大批量的 InSAR 形变解译。目前很多研究开展了基于 InSAR 形变速率以及干涉图的地震、滑坡相关信号探测的研究[119-122],通过建立专家知识库训练卷积神经网络模型,实现在 InSAR 形变结果中准确探测相关灾害信号的位置。城市场景下涉及的形变类型多样,城市场景下利用深度学习模型开展智能识别相对复杂。Wu 等[106]引入面向对象的循环神经网络方法识别建筑物、滑坡、农田、鱼塘、吹填工程等相关形变信号的识别。时序 InSAR 技术提供了相干点序列的形变信息,从时间序列形变的特征,同样能提供形变模式的重要信息。Kulshrestha 等[123]使用长短期记忆递归神经网络(long short term memory, LSTM)分类模型识别与地表塌陷相关的阶梯型和分段型两种异常形变序列。Lattari 等[124]同样基于 LSTM 模型实现时序形变异常转变时刻点的探测。未来多平台、多波段、多极化、多分辨率、多角度的 SAR 数据提供了地表丰富的信息数据,如何自动挖掘 InSAR 形变数据的语义知识仍是关注热点。

2.3　基于时序 InSAR 相干点散射机制的形变解译

InSAR 相干点的几何参数、语义信息能帮助形变信号的解译,但 InSAR 信号的散射机制也是不可忽略的部分。三维坐标确定了 InSAR 相干点的空间最优几何位置,但可能在物理上不是现实存在的。例如,由地物与地表多次散射形成的点目标,几何定位的结果可能会是在地下的重影散射信号。而散射机制描述了电磁波与地物之间的相互作用,与语义信息相互补充,能辅助形变信号解译。

InSAR 相干点的散射机制提供地物识别的重要信息,目前研究主要集中于两方面:一方面,基于散射机理的全极化数据目标分解,通过测量目标散射描述以深入理解其物理特性,服务于地物的识别。另一方面,基于 SAR 目标散射信号的模拟,通过对目标信号成像过程的追踪,实现目标信息刻画。

电磁波极化对目标物理散射特性敏感,通过极化散射矩阵的分解可以提供地物散射类型特征。目前极化分解领域内算法很多,基本可以分为相干分解和非/部分相干分解两类。相干分解通过目标散射矩阵分解为基本的散射形式获得观测目标的物理结构,包含的算法有

Pauli分解[125]、SDH(sphere dihedral helix)分解[126]、Cameron分解[127]、SSCM(symmetric scattering characterization method)分解[128]等。Pauli分解将目标散射分解为奇次散射、偶次散射、旋转二面角散射和非对称散射。SDH分解将目标分为球、二面角、螺旋体的组合。Cameron根据互易性和对称性来区分目标类型,SSCM在Cameron基础上提出了一种散射相似评估方法。非相干/部分相干分解则是将目标极化相干矩阵、极化协方差矩阵、Mueller或Kennaugh矩阵分解为简单或标准二阶描述的组合,并给出物理解释,包括Huynen分解[129]、Holm-Barnes分解[130]、Cloude分解[125]、Freeman-Durden分解[131]。Huynen二分分解法将任一目标Stokes矩阵表示为一个确定目标和分布目标Stokes矩阵之和,可以用任意9个独立参数描述目标的物理特性。Holm-Barnes分解根据空间向量理论进一步扩展,将任意非稳态目标分解为唯一的主导稳态目标、完全非极化波以及残留项。Cloude分解是基于特征分析方法提出的,将大量的极化信息压缩为表达散射机理的3个非负特征值。Freeman认为这3个散射值难以与物理散射模型建立关联,进一步提出三分量分解法,利用极化协方差/相干矩阵建立三种模型:体散射、二次散射、表面或者单次散射。

借助于极化数据,许多研究者开展了城市场景InSAR相干点的散射机制及其辅助形变解译的研究。Van Zyl等[132]研究发现城市地区的散射分类与偶数反射类的散射相似。Dong等[133]发现城市环境中的后向散射来源十分复杂,主要来自于屋顶一次散射,并且后向散射与入射角有很大的关联。综合几何参数、散射机制、语义信息能实现InSAR形变信号的深度解译。Ketelaar等[134]在荷兰鹿特丹地区的应用研究中通过对散射机制的分析定义三种不同的变形类型,从而识别不同的变形驱动机制。Dheenathayalan等[135]联合极化数据、高程数据和幅度数据,将InSAR相干点分为了六类:地面单面体、高架单面体、地面双面体、高架双面体、二面体极点和地面三面体。Chang等[136]利用极化数据提取了InSAR散射信息,同时引入土地利用数据,实现联合多源数据的InSAR形变机制解析。未来多极化的SAR数据能提供地物目标丰富的散射机制信息,如何利用散射机制信息联合InSAR所探测的形变信号,实现形变机制的解译是未来的挑战。

SAR信号模拟的方法也提供了一种对于InSAR相干点散射机制理解的解决思路[110]。SAR信号和图像的模拟被广泛应用在雷达系统测试、雷达图形几何纠正、雷达图像解译和新算法测试等[137-139]。目前的SAR模拟软件包括但不限于SARAS[140-141]、Pol-SARAS[142]、CAS[143]、Xpatch4[144]、GRECOSAR[145]、CohRaS[146]、SARViz[147]以及RaySAR[148]等。表2整理了当下主流模拟器的特性对比。SARAS和CAS面向海洋应用,不考虑复杂目标的多重散射。Pol-SARAS是SARAS的极化版本,它考虑了自然场景的模拟[142]。Xpatch4是Xpatch的一个面向对象版本,它提供了0D雷达截面、1D距离剖面、2D SAR图像和3D散射中心特征,它是基于光纤的发射和反弹机制开发的,支持并行计算[144]。Xpatch已广泛用于飞行器的研究,通常是飞机或地面飞行器[149-151]。GRECOSAR可以生成复杂目标的极化SAR和逆极化SAR影像,并被广泛用于船舶分类研究[145]。CohRaS是一个基于光线跟踪的SAR模拟器,主要用于高分辨率的小场景,它仅支持由凸多边形构成的几何体作为观测模型[146]。SARViz是一个利用3D硬件加速和可编程图形处理器显卡实现的SAR图像模拟系统,它只模拟单次和双次反弹反射,不考虑多个回波的相干叠加[147]。RaySAR是基于光线跟踪的SAR图像模拟器,它是在开源软件POVRay上引入的SAR成像集合模型并且功能强大的模拟器,主要面向理解复杂城市场景目标的图像[148,152-154]。

基于Ray-Tracing的三维SAR信号模拟器存在一些限制,但是比较适合应用于理解城市区域的相干点散射机制:(1)它可以处理任意数量的散射次数;(2)它能保持追踪单个散射信号的形成路径;(3)它提供形成的相干点的三维位置和散射次数;(4)它是开放获得的并且计算成本低,可以模拟相对较大和复杂的城市场景。因此,上述的模拟器RaySAR被广泛用于城市场景中相干点散射机制的理解。

基于Ray-Tracing的三维模拟方法,学者们开展了城市场景中相干点的散射机制解读和分析,促进了对城市场景中相干点散射机制的理解。Auer等[153]通过RaySAR分析了由于多次散射引起的定位在地面以下的重影散射点的形成

机理及其特点。Auer和Gernhardt[154]指出线性地物一般认为是单次和二次散射引起的,实际上由于场景的复杂性,多数是三次散射信号。Auer等[155]结合模拟给出一种针对规则分布的由窗户形成的建筑立面的叠掩信号利用的方法。张月婷等[156]基于Ray-Tracing的方法分析了单个大型建筑物桥梁的散射特性。Gernhardt等[77]结合RaySAR实现了InSAR相干点的精度分析与建筑物立面的关联。赵婧文等[157]模拟和分析了上海外滩建筑物的信号。Yang等[110]讨论了不同细节程度的城市模型对相干点模拟的影响,实现了InSAR和建筑模型的关联,并且指出了城市中多次散射的普遍存在性。针对高分辨率影像中多次散射特性的分析也是一个研究热点[158-159]。

表 2　典型的SAR信号模拟软件特性对比

Tab. 2　Comparison of Typical SAR Simulation Software Characteristics

软件	处理类型	应用领域	散射类型	信号反射模型	模拟结果	速度	免费	极化
SARAS[140-141]	光线追踪	海洋	单次散射	几何光学(geometrical optics, GO)/物理光学(physical optics, PO)	原始信号	—	否	否
Pol-SARAS [142]	光线追踪	海洋/自然地物	单次散射	GO/PO	原始信号	—	否	是
CSA[143]	—	海洋	单次散射	GO/PO	原始信号	—	否	是
Xpatch4[144]	光线追踪	飞机/车辆	单次/多次	PO/物理衍射理论	聚焦影像	—	是	否
GRECOSAR[145]	高频处理	人工目标/舰船	单次/多次	PO/物理衍射理论	原始信号	—	否	是
CohRaS[146]	光线追踪	目标分类	单次/多次	双重模型	聚焦影像	中等	否	是
SARViz[147]	光栅法	实时模拟	单次/二次	着色描影	聚焦影像	快速	否	否
RaySAR[148]	光线追踪	城市目标	单次/多次	着色描影	聚焦影像	超快速	是	否

InSAR相干点的散射机制和精确的位置对其测量形变信号的解译也十分重要。Yang[160]提出散射次数影响了真实形变在点目标上观测的形变的表达,通过模拟单个建筑物沿着雷达视线方向(line of sight, LOS)沉降 1 mm 的事件,其结果如图4所示,其中1~9号点来源于窗户角点的三次散射,散射相位中心与形变的建筑体一同变化,因此探测形变量一致。相反,10~16号点来自于建筑物和地面的三次散射,由于散射相位中心没有变化,因此没有探测到形变量。图4中的五次散射点目标17~23号,由于多次散射的长传播途径形成的重影散射,其观测的形变量与真实形变量相反。从模拟的建筑物下沉案例可知,23个模拟点中,1~9号点表达了下沉形变事件,10~16号点表达了稳定状态,17~23号给出的是相反的运动状态。在真实观测场景下,忽略相干点所在的位置和散射次数的形变分析,可能会得出这个建筑物局部结构不均匀沉降或者地表出现抬升这样的错误判断。

当前的InSAR结果解译时,引入InSAR相干点的位置和散射特性对其形变表达的影响的考虑,可能帮助避免形变信号的错误解读。InSAR相干点的散射机制的理解不仅有助于确定其与地物的关联,更对于形变信号解译很重要。未来联合SAR信号散射机理开展城市目标地物参数反演以及形变机制解译仍然是热点问题。

3　结　语

在过去的数十年里,时间序列InSAR技术已被广泛应用于城市场景的形变监测。然而,对于复杂城市场景的InSAR精细监测以及形变信号解译仍然是当前和未来面临的挑战,对于拓展InSAR技术应用的深度和广度有着重要意义。本文总结了建立InSAR相干点-地物目标-观测场景之间关联的关键参数,主要包括运动学特征、几何参数、语义信息和物理属性。在这个思路上,综述了InSAR相干点相关参数提取以及基于参数提取开展的形变解译研究。

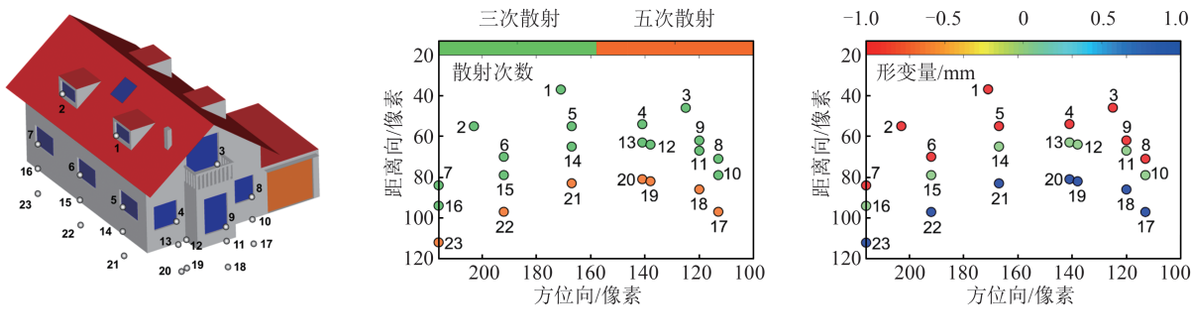

(a) 单个建筑物上模拟的InSAR强散射点目标　(b) 点目标的散射次数,包含三次散射和五次散射　(c) 点目标上的LOS变量

图4　文献[160]模拟单个建筑物下沉事件所探测的InSAR相干点位置、散射次数及其沿着LOS方向形变量

Fig. 4　InSAR Coherent Point Positions, Bounce Level, and the Detected Displacements Along the LOS Direction Under the Simulation of the Sinking of a Single Building in Reference [160]

在城市场景中进行InSAR精细监测时,高精度的三维定位是重要的基础数据。它不仅有助于确定形变信号的来源,且利于形变机制的分析。借助于三维模型、高分辨率光学影像、激光点云数据和土地利用数据等语义信息来辅助InSAR形变解译是一种思路。另一方面,基于InSAR形变数据驱动的语义信息挖掘结合深度学习也是当前的发展热点。在城市环境中,地物目标的散射机制复杂,多次散射信号不仅能提供有效的形变观测,还能提供关于目标尺寸的信息。如何联合SAR信号散射机理开展城市目标地物参数反演和形变机制解译仍然是亟待解决的难题。在InSAR相干点几何参数、语义信息和物理属性的框架下,综合形变解译与机制认知,最终将服务于未来城市场景精细智能形变监测、识别和安全评估等应用。

参 考 文 献

[1] Ferretti A, Prati C, Rocca F. Permanent Scatterers in SAR Interferometry[J]. *IEEE Transactions on Geoscience and Remote Sensing*, 2001, 39(1): 8-20.

[2] Berardino P, Fornaro G, Lanari R, et al. A New Algorithm for Surface Deformation Monitoring Based on Small Baseline Differential SAR Interferograms[J]. *IEEE Transactions on Geoscience and Remote Sensing*, 2002, 40(11): 2375-2383.

[3] Hooper A, Zebker H, Segall P, et al. A New Method for Measuring Deformation on Volcanoes and Other Natural Terrains Using InSAR Persistent Scatterers[J]. *Geophysical Research Letters*, 2004, 31(23): L23611.

[4] Kampes B M. Radar Interferometry: Persistent Scatterer Technique[M]. Dordrecht, the Netherlands: Springer, 2006.

[5] Ferretti A, Fumagalli A, Novali F, et al. A New Algorithm for Processing Interferometric Data-Stacks: SqueeSAR[J]. *IEEE Transactions on Geoscience and Remote Sensing*, 2011, 49(9): 3460-3470.

[6] Minh D, Hanssen R, Rocca F. Radar Interferometry: 20 Years of Development in Time Series Techniques and Future Perspectives[J]. *Remote Sensing*, 2020, 12(9): 1364.

[7] Li Deren, Liao Mingsheng, Wang Yan. Progress of Permanent Scatterer Interferometry[J]. *Geomatics and Information Science of Wuhan University*, 2004, 29(8): 664-668. (李德仁, 廖明生, 王艳. 永久散射体雷达干涉测量技术[J]. 武汉大学学报(信息科学版), 2004, 29(8): 664-668.)

[8] Guo L, Gong H, Li J, et al. Understanding Uneven Land Subsidence in Beijing, China, Using a Novel Combination of Geophysical Prospecting and InSAR[J]. *Geophysical Research Letters*, 2020, 47(16): e2020GL088676.

[9] Dong J, Guo S, Wang N, et al. Tri-decadal Evolution of Land Subsidence in the Beijing Plain Revealed by Multi-Epoch Satellite InSAR Observations[J]. *Remote Sensing of Environment*, 2023, 286: 113446.

[10] Luo Q L, Perissin D, Zhang Y Z, et al. L- and X-band Multi-temporal InSAR Analysis of Tianjin Subsidence[J]. *Remote Sensing*, 2014, 6(9): 7933-7951.

[11] Shi X G, Zhu T T, Tang W, et al. Inferring Decelerated Land Subsidence and Groundwater Storage Dynamics in Tianjin - Langfang Using Sentinel-1 InSAR[J]. *International Journal of Digital Earth*, 2022, 15(1): 1526-1546.

[12] Wang R, Yang M S, Yang T L, et al. Decomposing and Mapping Different Scales of Land Subsidence over Shanghai with X- and C-Band SAR Data Stacks[J]. *International Journal of Digital Earth*, 2022, 15(1): 478-502.

[13] Liao Mingsheng, Pei Yuanyuan, Wang Hanmei, et al. Subsidence Monitoring in Shanghai Using the PSInSAR Technique[J]. *Shanghai Land & Resources*, 2012, 33(3): 5-10. (廖明生, 裴媛媛, 王寒梅, 等. 永久散射体雷达干涉技术监测上海地面沉降[J]. 上海国土资源, 2012, 33(3): 5-10.)

[14] Wang Yan, Liao Mingsheng, Li Deren, et al. Subsidence Velocity Retrieval from Long-term Coherent Targets in Radar Interferometric Stacks[J]. *Chinese Journal of Geophysics*, 2007, 50(2): 598-604. (王艳, 廖明生, 李德仁, 等. 利用长时间序列相干目标获取地面沉降场[J]. 地球物理学报, 2007, 50(2): 598-604.)

[15] Zhang Qin, Zhao Chaoying, Ding Xiaoli, et al. Research on Recent Characteristics of Spatio-temporal Evolution and Mechanism of Xi'an Land Subsidence and Ground Fissure by Using GPS and InSAR Techniques[J]. *Chinese Journal of Geophysics*, 2009, 52(5): 1214-1222. (张勤, 赵超英, 丁晓利, 等. 利用GPS与InSAR研究西安现今地面沉降与地裂缝时空演化特征[J]. 地球物理学报, 2009, 52(5): 1214-1222.)

[16] Li G, Zhao C, Wang B, et al. Evolution of Spatio-temporal Ground Deformation over 30 Years in Xi'an, China, with Multi-sensor SAR Interferometry[J]. *Journal of Hydrology*, 2023, 616: 128764.

[17] Tang W, Liao M. Taiyuan City Subsidence Observed with Persistent Scatterer InSAR[J]. *Wuhan University Journal of Natural Sciences*, 2014, 19(6): 526-534.

[18] Liu Y, Zhao C, Zhang Q, et al. Land Subsidence in Taiyuan, China, Monitored by InSAR Technique With Multisensor SAR Datasets From 1992 to 2015[J]. *IEEE Journal of Selected Topics in Applied Earth Observations and Remote Sensing*, 2018, 11(5): 1509-1519.

[19] Ng A, Wang H, Dai Y, et al. InSAR Reveals Land Deformation at Guangzhou and Foshan, China Between 2011 and 2017 with COSMO-SkyMed Data[J]. *Remote Sensing*, 2018, 10(6): 813.

[20] Sun M, Du Y, Liu Q, et al. Understanding the Spatial-Temporal Characteristics of Land Subsidence in Shenzhen Under Rapid Urbanization Based on MT-InSAR[J]. *IEEE Journal of Selected Topics in Applied Earth Observations and Remote Sensing*, 2023, 16: 4153-4166.

[21] Xu B, Feng G, Li Z, et al. Coastal Subsidence Monitoring Associated with Land Reclamation Using the Point Target Based SBAS-InSAR Method: A Case Study of Shenzhen, China[J]. *Remote Sensing*, 2016, 8(8): 652-670.

[22] Bai Lin, Jiang Liming, Wang Hansheng. Monitoring Ground Subsidence in Wuhan City with High-Resolution TerraSAR-X Images from 2013 to 2015[J]. *Journal of Geodesy and Geodynamics*, 2019, 39(8): 832-836. (白林, 江利明, 汪汉胜. 利用高分辨率TerraSAR-X数据监测武汉地区2013—2015年地面沉降[J]. 大地测量与地球动力学, 2019, 39(8): 832-836.)

[23] Shi X, Zhang S, Jiang M, et al. Spatial and Temporal Subsidence Characteristics in Wuhan (China), During 2015 - 2019, Inferred from Sentinel-1 Synthetic Aperture Radar (SAR) Interferometry[J]. *Natural Hazards and Earth System Sciences*, 2021, 21(8): 2285-2297.

[24] Zhang Y, Zhang J, Wu H, et al. Monitoring of Urban Subsidence with SAR Interferometric Point Target Analysis: A Case Study in Suzhou, China[J]. *International Journal of Applied Earth Observation and Geoinformation*, 2011, 13(5): 812-818.

[25] Shi G, Ma P, Hu X, et al. Surface Response and Subsurface Features During the Restriction of Groundwater Exploitation in Suzhou (China) Inferred from Decadal SAR Interferometry[J]. *Remote Sensing of Environment*, 2021, 256: 112327.

[26] Zhou C, Lan H, Bürgmann R, et al. Application of an Improved Multi-temporal InSAR Method and Forward Geophysical Model to Document Subsidence and Rebound of the Chinese Loess Plateau Following Land Reclamation in the Yan'an New District[J]. *Remote Sens Environ*, 2022, 279:113102.

[27] Wang Y D, Feng G C, Li Z W, et al. Estimating the Long-term Deformation and Permanent Loss of Aquifer in the Southern Junggar Basin, China, Using InSAR[J]. *Journal of Hydrology*, 2022, 614: 128604.

[28] Li P, Wang G, Liang C, et al. InSAR-Derived Coastal Subsidence Reveals New Inundation Scenarios over the Yellow River Delta[J]. *IEEE Journal of Selected Topics in Applied Earth Observations and Remote Sensing*, 2023, DOI: 10.1109/JSTARS.2023.32724782.

[29] Zhao Q, Lin H, Gao W, et al. InSAR Detection of Residual Settlement of an Ocean Reclamation Engineering Project: A Case Study of Hong Kong Inter-

national Airport [J]. *Journal of Oceanography*, 2011, 67(4): 415-426.

[30] Jiang Y N, Liao M S, Wang H M, et al. Deformation Monitoring and Analysis of the Geological Environment of Pudong International Airport with Persistent Scatterer SAR Interferometry [J]. *Remote Sensing*, 2016, 8(12): 1021.

[31] Marshall C, Large D J, Athab A, et al. Monitoring Tropical Peat Related Settlement Using ISBAS InSAR, Kuala Lumpur International Airport (KLIA) [J]. *Engineering Geology*, 2018, 244: 57-65.

[32] Bianchini Ciampoli L, Gagliardi V, Ferrante C, et al. Displacement Monitoring in Airport Runways by Persistent Scatterers SAR Interferometry [J]. *Remote Sensing*, 2020, 12(21): 3564.

[33] Wu S B, Yang Z F, Ding X L, et al. Two Decades of Settlement of Hong Kong International Airport Measured with Multi-temporal InSAR [J]. *Remote Sensing of Environment*, 2020, 248: 111976.

[34] An B, Jiang Y, Wang C, et al. Ground Infrastructure Monitoring in Coastal Areas Using Time-Series InSAR Technology: The Case Study of Pudong International Airport, Shanghai [J]. *International Journal of Digital Earth*, 2023, 16(1): 2171144.

[35] Huang Q, Crosetto M, Monserrat O, et al. Displacement Monitoring and Modelling of a High-Speed Railway Bridge Using C-band Sentinel-1 Data [J]. *ISPRS Journal of Photogrammetry and Remote Sensing*, 2017, 128: 204-211.

[36] Lazecky M, Hlavacova I, Bakon M, et al. Bridge Displacements Monitoring Using Space-Borne X-Band SAR Interferometry [J]. *IEEE Journal of Selected Topics in Applied Earth Observations and Remote Sensing*, 2017, 10(1): 205-210.

[37] Peduto D, Elia F, Montuori R. Probabilistic Analysis of Settlement-Induced Damage to Bridges in the City of Amsterdam (The Netherlands) [J]. *Transportation Geotechnics*, 2018, 14: 169-182.

[38] Qin X Q, Zhang L, Yang M S, et al. Mapping Surface Deformation and Thermal Dilation of Arch Bridges by Structure-Driven Multi-temporal DInSAR Analysis [J]. *Remote Sensing of Environment*, 2018, 216: 71-90.

[39] Ma P F, Li T, Fang C Y, et al. A Tentative Test for Measuring the Sub-millimeter Settlement and Uplift of a High-Speed Railway Bridge Using COSMO-SkyMed Images [J]. *ISPRS Journal of Photogrammetry and Remote Sensing*, 2019, 155: 1-12.

[40] Milillo P, Giardina G, Perissin D, et al. Pre-Collapse Space Geodetic Observations of Critical Infrastructure: The Morandi Bridge, Genoa, Italy [J]. *Remote Sensing*, 2019, 11(12): 1403-1403.

[41] Xiong S T, Wang C S, Qin X Q, et al. Time-series Analysis on Persistent Scatter-Interferometric Synthetic Aperture Radar (PS-InSAR) Derived Displacements of the Hong Kong - Zhuhai - Macao Bridge (HZMB) from Sentinel-1A Observations [J]. *Remote Sensing*, 2021, 13(4): 546-558.

[42] Chen F, Lin H, Li Z, et al. Interaction Between Permafrost and Infrastructure Along the Qinghai-Tibet Railway Detected via Jointly Analysis of C- and L-band Small Baseline SAR Interferometry [J]. *Remote Sensing of Environment*, 2012, 123: 532-540.

[43] Chang L, Dollevoet R, Hanssen R. Nationwide Railway Monitoring Using Satellite SAR Interferometry [J]. *IEEE Journal of Selected Topics in Applied Earth Observations and Remote Sensing*, 2017, 10(2): 596-604.

[44] Qin X Q, Liao M S, Zhang L, et al. Structural Health and Stability Assessment of High-speed Railways via Thermal Dilation Mapping with Time-Series InSAR Analysis [J]. *IEEE Journal of Selected Topics in Applied Earth Observations and Remote Sensing*, 2017, 10(6): 2999-3010.

[45] Xing X, Zhu Y, Xu W, et al. Measuring Subsidence over Soft Clay Highways Using a Novel Time-series InSAR Deformation Model with an Emphasis on Rheological Properties and Environmental Factors (NREM) [J]. *IEEE Transactions on Geoscience and Remote Sensing*, 2022, 60: 1-19.

[46] Shi X, Jiang L, Jiang H, et al. Geohazards Analysis of the Litang-Batang Section of Sichuan-Tibet Railway Using SAR Interferometry [J]. *IEEE Journal of Selected Topics in Applied Earth Observations and Remote Sensing*, 2021, 14: 11998-12006.

[47] Perissin D, Wang Z, Lin H. Shanghai Subway Tunnels and Highways Monitoring Through Cosmo-SkyMed Persistent Scatterers [J]. *ISPRS Journal of Photogrammetry and Remote Sensing*, 2012, 73: 58-67.

[48] Li T, Liu G, Lin H, et al. Detecting Land Subsidence near Metro Lines in the Baoshan District of

Shanghai with Multi-temporal Interferometric Synthetic Aperture Radar [J]. *Journal of Modern Transportation*, 2014, 22(3): 137-147.

[49] Wang H, Feng G, Xu B, et al. Deriving Spatio-temporal Development of Ground Subsidence due to Subway Construction and Operation in Delta Regions with PS-InSAR Data: A Case Study in Guangzhou, China[J]. *Remote Sensing*, 2017, 9(10): 1004.

[50] Giardina G, Milillo P, Dejong M, et al. Evaluation of InSAR Monitoring Data for Post-Tunnelling Settlement Damage Assessment[J]. *Structural Control and Health Monitoring*, 2019, 26(2): e2285.

[51] Macchiarulo V, Milillo P, DeJong M J, et al. Integrated InSAR Monitoring and Structural Assessment of Tunnelling-Induced Building Deformations [J]. *Structural Control and Health Monitoring*, 2021, 28(9): e2781.

[52] Reinders K J, Hanssen R F, van Leijen F J, et al. Augmented Satellite InSAR for Assessing Short-Term and Long-Term Surface Deformation due to Shield Tunnelling [J]. *Tunnelling and Underground Space Technology*, 2021, 110: 103745.

[53] Wu S, Zhang B, Liang H, et al. Detecting the Deformation Anomalies Induced by Underground Construction Using Multiplatform MT-InSAR: A Case Study in to Kwa Wan Station, Hong Kong [J]. *IEEE Journal of Selected Topics in Applied Earth Observations and Remote Sensing*, 2021, 14: 9803-9814.

[54] Wang R, Yang M, Dong J, et al. Investigating Deformation Along Metro Lines in Coastal Cities Considering Different Structures with InSAR and SBM Analyses [J]. *International Journal of Applied Earth Observation and Geoinformation*, 2022, 115: 103099.

[55] Yang M, Wang R, Li M, et al. A PSI Targets Characterization Approach to Interpreting Surface Displacement Signals: A Case Study of the Shanghai Metro Tunnels[J]. *Remote Sensing of Environment*, 2022, 280: 113150.

[56] Zeni G, Bonano M, Casu F, et al. Long-term Deformation Analysis of Historical Buildings Through the Advanced SBAS-DInSAR Technique: The Case Study of the City of Rome, Italy[J]. *Journal of Geophysics and Engineering*, 2011, 8(3): S1-S12.

[57] Gernhardt S, Bamler R. Deformation Monitoring of Single Buildings Using Meter-Resolution SAR Data in PSI[J]. *ISPRS Journal of Photogrammetry and Remote Sensing*, 2012, 73: 68-79.

[58] Chang L, Hanssen R F. Detection of Cavity Migration and Sinkhole Risk Using Radar Interferometric Time Series[J]. *Remote Sensing of Environment*, 2014, 147: 56-64.

[59] Ma P, Lin H, Lan H, et al. Multi-dimensional SAR Tomography for Monitoring the Deformation of Newly Built Concrete Buildings[J]. *ISPRS Journal of Photogrammetry and Remote Sensing*, 2015, 106: 118-128.

[60] Chen F, Wu Y, Zhang Y, et al. Surface Motion and Structural Instability Monitoring of Ming Dynasty City Walls by Two-step Tomo-PSInSAR Approach in Nanjing City, China[J]. *Remote Sensing*, 2017, 9(4): 371.

[61] Wang Z, Balz T, Zhang L, et al. Using TSX/TDX Pursuit Monostatic SAR Stacks for PS-InSAR Analysis in Urban Areas [J]. *Remote Sensing*, 2018, 11(1): 26.

[62] Liu P, Li Z, Wang C, et al. Phase Unmixing of TerraSAR-X Staring Spotlight Interferograms in Building Scale for PS Height and Deformation[J]. *ISPRS Journal of Photogrammetry and Remote Sensing*, 2021, 180: 14-28.

[63] Ma P, Zheng Y, Zhang Z, et al. Building Risk Monitoring and Prediction Using Integrated Multi-temporal InSAR and Numerical Modeling Techniques[J]. *International Journal of Applied Earth Observation and Geoinformation*, 2022, 114: 103076.

[64] Bassoli E, Vincenzi L, Grassi F, et al. A Multi-temporal DInSAR-based Method for the Assessment of the 3D Rigid Motion of Buildings and Corresponding Uncertainties[J]. *Journal of Building Engineering*, 2023, 73: 106738.

[65] Xing Mengdao, Lin Hao, Chen Jianlai, et al. A Review of Imaging Algorithms in Multi-Platform-Borne Synthetic Aperture Radar[J]. *Journal of Radars*, 2019, 8(6): 732-757. (邢孟道, 林浩, 陈溅来, 等. 多平台合成孔径雷达成像算法综述[J]. 雷达学报, 2019, 8(6): 732-757.)

[66] Liao Mingsheng, Wang Ru, Yang Mengshi, et al. Techniques and Applications of Spaceborne Time-Series InSAR in Urban Dynamic Monitoring [J]. *Journal of Radars*, 2020, 9(3): 409-424. (廖明生, 王茹, 杨梦诗, 等. 城市目标动态监测中的时序 InSAR 分析方法及应用[J]. 雷达学报, 2020, 9(3): 409-424.)

[67] Zhu Jianjun, Song Yingchun, Hu Jun, et al. Challenges and Development of Data Processing Theory

in the Era of Surveying and Mapping Big Data[J]. *Geomatics and Information Science of Wuhan University*, 2021, 46(7): 1025-1031. (朱建军, 宋迎春, 胡俊, 等. 测绘大数据时代数据处理理论面临的挑战与发展[J]. 武汉大学学报(信息科学版), 2021, 46(7): 1025-1031.)

[68] Ge Daqing, Dai Keren, Guo Zhaocheng, et al. Early Identification of Serious Geological Hazards with Integrated Remote Sensing Technologies: Thoughts and Recommendations[J]. *Geomatics and Information Science of Wuhan University*, 2019, 44(7): 949-956. (葛大庆, 戴可人, 郭兆成, 等. 重大地质灾害隐患早期识别中综合遥感应用的思考与建议[J]. 武汉大学学报(信息科学版), 2019, 44(7): 949-956.)

[69] Dheenathayalan P, Small D, Schubert A, et al. High-Precision Positioning of Radar Scatterers[J]. *Journal of Geodesy*, 2016, 90(5): 403-422.

[70] Small D, Rosich B, Meier E, et al. Geometric Calibration and Validation of ASAR Imagery [C]// CEOS SAR Workshop, Ulm,Geimany, 2004.

[71] Schubert A, Jehle M, Small D, et al. Influence of Atmospheric Path Delay on the Absolute Geolocation Accuracy of TerraSAR-X High-Resolution Products[J]. *IEEE Transactions on Geoscience and Remote Sensing*, 2010, 48(2): 751-758.

[72] Eineder M, Minet C, Steigenberger P, et al. Imaging Geodesy-Toward Centimeter-Level Ranging Accuracy with TerraSAR-X[J]. *IEEE Transactions on Geoscience and Remote Sensing*, 2011, 49(2): 661-671.

[73] Cong X, Balss U, Eineder M, et al. Imaging Geodesy-Centimeter-Level Ranging Accuracy with TerraSAR-X: An Update[J]. *IEEE Geoscience and Remote Sensing Letters*, 2012, 9(5): 948-952.

[74] Balss U, Gisinger C, Eineder M. Measurements on the Absolute 2-D and 3-D Localization Accuracy of TerraSAR-X [J]. *Remote Sensing*, 2018, 10(4): 656.

[75] Schubert A, Miranda N, Geudtner D, et al. Sentinel-1A/B Combined Product Geolocation Accuracy [J]. *Remote Sensing*, 2017, 9(6): 607.

[76] Gisinger C, Schubert A, Breit H, et al. In-Depth Verification of Sentinel-1 and TerraSAR-X Geolocation Accuracy Using the Australian Corner Reflector Array[J]. *IEEE Transactions on Geoscience and Remote Sensing*, 2021, 59(2): 1154-1181.

[77] Gernhardt S, Auer S, Eder K. Persistent Scatterers at Building Facades-Evaluation of Appearance and Localization Accuracy[J]. *ISPRS Journal of Photogrammetry and Remote Sensing*, 2015, 100: 92-105.

[78] Zhou Yueqin, Zheng Zhaobao, Li Deren, et al. Stereopair Positioning Algorithm for SAR Images and Its Accuracy Analysis ModelSAR[J]. *Journal of Remote Sensing*, 1998, 4(2): 245-250. (周月琴, 郑肇葆, 李德仁, 等. SAR图像立体定位原理与精度分析[J]. 遥感学报, 1998, 4(2): 245-250.)

[79] Gernhardt S, Cong X, Eineder M, et al. Geometrical Fusion of Multitrack PS Point Clouds[J]. *IEEE Geoscience and Remote Sensing Letters*, 2012, 9(1): 38-42.

[80] Gisinger C, Balss U, Pail R, et al. Precise Three-Dimensional Stereo Localization of Corner Reflectors and Persistent Scatterers with TerraSAR-X [J]. *IEEE Transactions on Geoscience and Remote Sensing*, 2015, 53(4): 1782-1802.

[81] Duque S, Parizzi A, Zan F D, et al. Precise and Automatic 3D Absolute Geolocation of Targets Using only Two Long-Aperture SAR Acquisitions [C]. IEEE International Geoscience and Remote Sensing Symposium, Beijing,China,2016.

[82] Zhu X X, Montazeri S, Gisinger C, et al. Geodetic SAR Tomography[J]. *IEEE Transactions on Geoscience and Remote Sensing*, 2016, 54(1): 18-35.

[83] Zhu X, Bamler R. Very High Resolution Spaceborne SAR Tomography in Urban Environment[J]. *IEEE Transactions on Geoscience and Remote Sensing*, 2010, 48(12): 4296-4308.

[84] Montazeri S, Rodríguez González F, Zhu X. Geocoding Error Correction for InSAR Point Clouds[J]. *Remote Sensing*, 2018, 10(10): 1523.

[85] Van Zyl J J. Calibration of Polarimetric Radar Images Using only Image Parameters and Trihedral Corner Reflector Responses[J]. *IEEE Transactions on Geoscience and Remote Sensing*, 1990, 28(3): 337-348.

[86] Sarabandi K, Chiu T C. Optimum Corner Reflectors for Calibration of Imaging Radars[J]. *IEEE Transactions on Antennas and Propagation*, 1996, 44(10): 1348-1361.

[87] Small D, Schubert A, Rosich B, et al. Geometric and Radiometric Correction of ESA SAR Products [C]//Envisat Symposium 2007, Montreux, Switzerland, 2007.

[88] Shimada M, Isoguchi O, Tadono T, et al. PALSAR Radiometric and Geometric Calibration[J]. *IEEE Transactions on Geoscience and Remote Sensing*, 2009, 47(12): 3915-3932.

[89] Hanssen R F. Radar Interferometry: Data Interpretation and Error Analysis[M]. Boston:Kluwer Academic Publishers, 2001.

[90] Shi X, Zhang L, Balz T, et al. Landslide Deformation Monitoring Using Point-Like Target Offset Tracking with Multi-mode High-Resolution TerraSAR-X Data[J]. *ISPRS Journal of Photogrammetry and Remote Sensing*, 2015, 105: 128-140.

[91] Xia Y, Kaufmann H, Guo X. Differential SAR Interferometry Using Corner Reflectors[C]//IEEE International Geoscience and Remote Sensing Symposium, Toronto, Canada, 2002.

[92] Mahapatra P S, Samiei-Esfahany S, Van Der Marel H, et al. On the Use of Transponders as Coherent Radar Targets for SAR Interferometry[J]. *IEEE Transactions on Geoscience and Remote Sensing*, 2014, 52(3): 1869-1878.

[93] Crosetto M, Monserrat O, Cuevas-González M, et al. Persistent Scatterer Interferometry: A Review [J]. *ISPRS Journal of Photogrammetry and Remote Sensing*, 2016, 115: 78-89.

[94] Ferretti A, Savio G, Barzaghi R, et al. Submillimeter Accuracy of InSAR Time Series: Experimental Validation [J]. *IEEE Transactions on Geoscience and Remote Sensing*, 2007, 45(5): 1142-1153.

[95] Marinkovic P, Ketelaar G, Van Leijen F, et al. InSAR Quality Control: Analysis of Five Years of Corner Reflector Time Series[C]//The 5th International Workshop on ERS/Envisat SAR Interferometry (FRINGE 2007), Frascati, Italy ,2007.

[96] Garthwaite M C. On the Design of Radar Corner Reflectors for Deformation Monitoring in Multi-frequency InSAR [J]. *Remote Sensing*, 2017, 9 (7): 648.

[97] Gisinger C, Willberg M, Balss U, et al. Differential Geodetic Stereo SAR with TerraSAR-X by Exploiting Small Multi-Directional Radar Reflectors [J]. *Journal of Geodesy*, 2017, 91(1): 53-67.

[98] Mahapatra P, Der Marel H V, Van Leijen F, et al. InSAR Datum Connection Using GNSS-Augmented Radar Transponders[J]. *Journal of Geodesy*, 2018, 92(1): 21-32.

[99] Yang M, López-Dekker P, Dheenathayalan P, et al. On the Value of Corner Reflectors and Surface Models in InSAR Precise Point Positioning [J]. *ISPRS Journal of Photogrammetry and Remote Sensing*, 2019, 158: 113-122.

[100] Gisinger C, Eineder M, Brcic R, et al. First Experiences with Active C-Band Radar Reflectors and Sentinel-1[C]//IEEE International Geoscience and Remote Sensing Symposium, Kuala Lumpur, Malaysia, 2020.

[101] Eineder M, Gisinger C, Brcic R, et al. Long Term Geodetic Monitoring Using Active C-Band Radar Transponders and Sentinel-1-First Results [C]// FRINGE 2021, Nice, France, 2021.

[102] Yang M, Dheenathayalan P, Chang L, et al. High-Precision 3D Geolocation of Persistent Scatterers with One Single-Epoch GCP and LiDAR DSM Data [C]//Living Planet Symposium, Prague, Czech Republic, 2016.

[103] Dheenathayalan P, Cuenca M, Hanssen R. Different Approaches for PSI Target Characterization For Monitoring Urban Infrastructure [C]//FRINGE 2011, Frascati, Italy, 2011.

[104] Wang R, Yang T, Yang M, et al. A Safety Analysis of Elevated Highways in Shanghai Linked to Dynamic Load Using Long-term Time-series of InSAR Stacks[J]. *Remote Sensing Letters*, 2019, 10 (12): 1133-1142.

[105] Wang Y, Zhu X X, Zeisl B, et al. Fusing Meter-Resolution 4-D InSAR Point Clouds and Optical Images for Semantic Urban Infrastructure Monitoring [J]. *IEEE Transactions on Geoscience and Remote Sensing*, 2017, 55(1): 14-26.

[106] Wu Z, Ma P, Zheng Y, et al. Automatic Detection and Classification of Land Subsidence in Deltaic Metropolitan Areas Using Distributed Scatterer InSAR and Oriented R-CNN[J]. *Remote Sensing of Environment*, 2023, 290: 113545.

[107] Chang L, Sakpal N, Elberink S, et al. Railway Infrastructure Classification and Instability Identification Using Sentinel-1 SAR and Laser Scanning Data [J]. *Sensors*, 2020, 20(24): 7108.

[108] Schunert A, Soergel U. Assignment of Persistent Scatterers to Buildings[J]. *IEEE Transactions on Geoscience and Remote Sensing*, 2016, 54 (6): 3116-3127.

[109] Sun Y, Montazeri S, Wang Y, et al. Automatic Registration of a Single SAR Image and GIS Building Footprints in a Large-Scale Urban Area [J]. *ISPRS Journal of Photogrammetry and Remote Sensing*, 2020, 170: 1-14.

[110] Yang M S, López-Dekker P, Dheenathayalan P, et al. Linking Persistent Scatterers to the Built Environment Using Ray Tracing on Urban Models[J]. *IEEE Transactions on Geoscience and Remote Sensing*, 2019, 57(8): 5764-5776.

[111] Solano-Rojas D, Wdowinski S, Cabral-Cano E, et al. Detecting Differential Ground Displacements of

Civil Structures in Fast-Subsiding Metropolises with Interferometric SAR and Band-Pass Filtering[J]. *Scientific Reports*, 2020, 10: 15460.

[112] Lu P, Casagli N, Catani F, et al. Persistent Scatterers Interferometry Hotspot and Cluster Analysis (PSI-HCA) for Detection of Extremely Slow-moving Landslides[J]. *International Journal of Remote Sensing*, 2012, 33(2): 466-489.

[113] Festa D, Bonano M, Casagli N, et al. Nation-Wide Mapping and Classification of Ground Deformation Phenomena Through the Spatial Clustering of P-SBAS InSAR Measurements: Italy Case Study[J]. *ISPRS Journal of Photogrammetry and Remote Sensing*, 2022, 189: 1-22.

[114] Schneider P J, Soergel U. Clustering Persistent Scatterer Points Based on a Hybrid Distance Metric[C]//German Conference on Pattern Recognition, Berlin, Germany, 2021.

[115] Li Z, Zhao R, Hu J, et al. InSAR Analysis of Surface Deformation over Permafrost to Estimate Active Layer Thickness Based on One-Dimensional Heat Transfer Model of Soils[J]. *Scientific Reports*, 2015, 5: 15542.

[116] Zhu M, Wan X, Fei B, et al. Detection of Building and Infrastructure Instabilities by Automatic Spatio-temporal Analysis of Satellite SAR Interferometry Measurements[J]. *Remote Sensing*, 2018, 10(11): 1816.

[117] Chang L, Hanssen R F. A Probabilistic Approach for InSAR Time-Series Postprocessing[J]. *IEEE Transactions on Geoscience and Remote Sensing*, 2016, 54(1): 421-430.

[118] Berti M, Corsini A, Franceschini S, et al. Automated Classification of Persistent Scatterers Interferometry Time Series[J]. *Natural Hazards and Earth System Sciences*, 2013, 13(8): 1945-1958.

[119] Anantrasirichai N, Biggs J, Albino F, et al. A Deep Learning Approach to Detecting Volcano Deformation from Satellite Imagery Using Synthetic Datasets[J]. *Remote Sensing of Environment*, 2019, 230: 111179.

[120] Rouet-Leduc B, Jolivet R, Dalaison M, et al. Autonomous Extraction of Millimeter-Scale Deformation in InSAR Time Series Using Deep Learning[J]. *Nature Communications*, 2021, 12(1): 6480.

[121] Liu Y, Yao X, Gu Z, et al. Study of the Automatic Recognition of Landslides by Using InSAR Images and the Improved Mask R-CNN Model in the Eastern Tibet Plateau[J]. *Remote Sensing*, 2022, 14(14): 3362.

[122] Li Zhenhong, Song Chuang, Yu Chen, et al. Application of Satellite Radar Remote Sensing to Landslide Detection and Monitoring: Challenges and Solutions[J]. *Geomatics and Information Science of Wuhan University*, 2019, 44(7): 967-979. (李振洪, 宋闯, 余琛, 等. 卫星雷达遥感在滑坡灾害探测和监测中的应用: 挑战与对策[J]. 武汉大学学报(信息科学版), 2019, 44(7): 967-979.)

[123] Kulshrestha A, Chang L, Stein A. Use of LSTM for Sinkhole-Related Anomaly Detection and Classification of InSAR Deformation Time Series[J]. *IEEE Journal of Selected Topics in Applied Earth Observations and Remote Sensing*, 2022, 15: 4559-4570.

[124] Lattari F, Rucci A, Matteucci M. A Deep Learning Approach for Change Points Detection in InSAR Time Series[J]. *IEEE Transactions on Geoscience and Remote Sensing*, 2022, 60: 1-16.

[125] Lee J S, Pottier E. Polarimetric Radar Imaging: From Basics to Applications[M]. London, New York: CRC Press, 2009.

[126] Krogager E. New Decomposition of the Radar Target Scattering Matrix[J]. *Electronics Letters*, 2002, 26(18): 1525-1527.

[127] Cameron W L, Youssef N N, Leung L K. Simulated Polarimetric Signatures of Primitive Geometrical Shapes[J]. *IEEE Transactions on Geoscience and Remote Sensing*, 1996, 34(3): 793-803.

[128] Touzi R, Charbonneau F. Characterization of Target Symmetric Scattering Using Polarimetric SARs[J]. *IEEE Transactions on Geoscience and Remote Sensing*, 2002, 40(11): 2507-2516.

[129] Huynen J R. Phenomenological Theory of Radar Targets[D]. Delft: Delft University of Technology, 1970.

[130] Holm W, Barnes R. On Radar Polarization Mixed Target State Decomposition Techniques[C]//IEEE National Radar Conference, Ann Arbor, USA, 2002.

[131] Freeman A, Durden S L. A Three-Component Scattering Model for Polarimetric SAR Data[J]. *IEEE Transactions on Geoscience and Remote Sensing*, 1998, 36(3): 963-973.

[132] Van Zyl J J. Unsupervised Classification of Scattering Behavior Using Radar Polarimetry Data[J]. *IEEE Transactions on Geoscience and Remote Sensing*, 1989, 27(1): 36-45.

[133] Dong Y, Forster B, Ticehurst C. Radar Backscatter Analysis for Urban Environments[J]. *International Journal of Remote Sensing*, 2010, 18(6):

1351-1364.

[134] Ketelaar V, Hanssen R. Separation of Different Deformation Regimes Using PS-InSAR Data [C]// FRINGE 2003, Frascati ,Italy, 2003.

[135] Dheenathayalan P, Hanssen R. Target Characterization and Interpretation of Deformation Using Persistent Scatterer Interferometry and Polarimetry [C]//The 5th International Workshop on Science and Applications of SAR Polarimetry and Polarimetric Interferometry, Frascati ,Italy,2011.

[136] Chang L, Kulshrestha A, Zhang B, et al. Extraction and Analysis of Radar Scatterer Attributes for PAZ SAR by Combining Time Series InSAR, PolSAR, and Land Use Measurements [J]. *Remote Sensing*, 2023, 15(6): 1571.

[137] Wu Tao, Wang Chao, Zhang Hong, et al. Spaceborne SAR Image Simulation Based on Image Characteristics[J]. *Journal of Remote Sensing*, 2007, 11(2): 214-220. (吴涛, 王超, 张红, 等. 基于图像特征的星载 SAR 图像模拟研究[J]. 遥感学报, 2007, 11(2): 214-220.)

[138] Wen Xiaoyang, Zhang Hong, Wang Chao. The High Resolution SAR Image Simulation and Analysis of the Damaged Building in Earthquake[J]. *Journal of Remote Sensing*, 2009, 13(1): 169-176. (温晓阳, 张红, 王超. 地震损毁建筑物的高分辨率 SAR 图像模拟与分析[J]. 遥感学报, 2009, 13(1): 169-176.)

[139] Wang Guojun, Shao Yun, Zhang Fengli. Review of SAR Image Simulation for Urban Buildings[J]. *Remote Sensing Information*, 2012, 27(4): 116-122. (王国军, 邵芸, 张风丽. 城市建筑物 SAR 图像模拟综述[J]. 遥感信息, 2012, 27(4): 116-122.)

[140] Franceschetti G, Migliaccio M, Riccio D, et al. SARAS: A Synthetic Aperture Radar (SAR) Raw Signal Simulator[J]. *IEEE Transactions on Geoscience and Remote Sensing*, 1992, 30(1): 110-123.

[141] Franceschetti G, Migliaccio M, Riccio D. On Ocean SAR Raw Signal Simulation [J]. *IEEE Transactions on Geoscience and Remote Sensing*, 1998, 36(1): 84-100.

[142] Di Martino G, Iodice A, Poreh D, et al. Pol-SARAS: A Fully Polarimetric SAR Raw Signal Simulator for Extended Soil Surfaces [J]. *IEEE Transactions on Geoscience and Remote Sensing*, 2018, 56(4): 2233-2247.

[143] Huang Y H, Seguin G, Sultan N. Multi-frequency and Multi-polarization SAR System Analysis with Simulation Software Developed at CSA[C]//IEEE International Geoscience and Remote Sensing Symposium, Singapore, 2002.

[144] Andersh D, Moore J, Kosanovich S, et al. Xpatch 4: The Next Generation in High Frequency Electromagnetic Modeling and Simulation Software[C]// IEEE International Radar Conference, Alexandria, USA, 2002.

[145] Margarit G, Mallorqui J J, Rius J M, et al. On the Usage of GRECOSAR, An Orbital Polarimetric SAR Simulator of Complex Targets, to Vessel Classification Studies[J]. *IEEE Transactions on Geoscience and Remote Sensing*, 2006, 44(12): 3517-3526.

[146] Hammer H, Schulz K. SAR-Simulation of Large Urban Scenes Using an Extended Ray Tracing Approach [C]//2011 Joint Urban Remote Sensing Event. Munich, Germany, 2011.

[147] Balz T, Stilla U. Hybrid GPU-based Single- and Double-Bounce SAR Simulation[J]. *IEEE Transactions on Geoscience and Remote Sensing*, 2009, 47(10): 3519-3529.

[148] Auer S, Hinz S, Bamler R. Ray-Tracing Simulation Techniques for Understanding High-Resolution SAR Images[J]. *IEEE Transactions on Geoscience and Remote Sensing*, 2010, 48(3): 1445-1456.

[149] Hazlett M, Andersh D J, Lee S W, et al. XPATCH: A High-Frequency Electromagnetic Scattering Prediction Code Using Shooting and Bouncing Rays [J]. *The International Society for Optical Engineering*, 1995, 2469: 266-275.

[150] Castelloe M W, Munson D C. 3-D SAR Imaging via High-Resolution Spectral Estimation Methods: Experiments with XPATCH [C]//International Conference on Image Processing, Washington, USA, 1997.

[151] Bhalla R, Lin L, Andersh D. A Fast Algorithm for 3D SAR Simulation of Target and Terrain Using Xpatch[C]//IEEE International Radar Conference, Arlington, USA, 2005.

[152] Auer S. 3D Synthetic Aperture Radar Simulation for Interpreting Complex Urban Reflection Scenarios [D]. München: Technische Universität München, 2011.

[153] Auer S, Gernhardt S, Bamler R. Ghost Persistent Scatterers Related to Multiple Signal Reflections [J]. *IEEE Geoscience and Remote Sensing Letters*, 2011, 8(5): 919-923.

[154] Auer S, Gernhardt S. Linear Signatures in Urban SAR Images—Partly Misinterpreted? [J]. *IEEE Geoscience and Remote Sensing Letters*, 2014, 11

(10):1762-1766.

[155] Auer S, Gisinger C, Tao J. Characterization of Facade Regularities in High-Resolution SAR Images [J]. *IEEE Transactions on Geoscience and Remote Sensing*, 2015, 53(5): 2727-2737.

[156] Zhang Yueting, Qiu Xiaolan, Ding Chibiao, et al. The Simulation and Characteristics Analysis on High Resolution SAR Images of Bridges[J]. *Journal of Radars*, 2015, 4(1): 78-83. (张月婷, 仇晓兰, 丁赤飚, 等. 高分辨率SAR图像桥梁目标仿真与特性分析[J]. 雷达学报, 2015, 4(1): 78-83.)

[157] Zhao Jingwen, Wu Jicang, Ding Xiaoli. Synthetic Aperture Radar Image Simulation of the Bund Building Group in Shanghai Based on RaySAR Software[J]. *Journal of Tongji University (Natural Science)*, 2018, 46(4): 557-564. (赵婧文, 伍吉仓, 丁晓利. 基于RaySAR软件的上海外滩建筑群合成孔径雷达图像模拟[J]. 同济大学学报(自然科学版), 2018, 46(4): 557-564.)

[158] Cheng R, Liang X, Zhang F, et al. Multipath Scattering of Typical Structures in Urban Areas [J]. *IEEE Transactions on Geoscience and Remote Sensing*, 2019, 57(1): 342-351.

[159] Lei S, Qiu X, Zhang Y, et al. Analysis of the Multipath Scattering Effects in High-Resolution SAR Images[J]. *IEEE Geoscience and Remote Sensing Letters*, 2020, 17(4): 616-620.

[160] Yang M S. From Radar to Reality. Associating Persistent Scatterers to Corresponding Objects [D]. Delft: Delft University of Technology, 2020.